OPEN ACCESS
IOP Publishing
Plasma Sources Science and Technology
Plasma Sources Sci. Technol. **27** (2018) 015017 (13pp)
https://doi.org/10.1088/1361-6595/aaa5d8

Streamer properties and associated x-rays in perturbed air

C Köhn[1,3], O Chanrion[1], L P Babich[2] and T Neubert[1]

[1] Technical University of Denmark, National Space Institute (DTU Space), Elektrovej 328, 2800 Kgs Lyngby, Denmark
[2] Russian Federal Nuclear Center—VNIIEF, Sarov, Russia

E-mail: koehn@space.dtu.dk, chanrion@space.dtu.dk, babich@elph.vniief.ru and neubert@space.dtu.dk

Received 3 August 2017, revised 18 December 2017
Accepted for publication 8 January 2018
Published 25 January 2018

Abstract

Streamers are ionization waves in electric discharges. One of the key ingredients of streamer propagation is an ambient gas that serves as a source of free electrons. Here, we explore the dependence of streamer dynamics on different spatial distributions of ambient air molecules. We vary the spatial profile of air parallel and perpendicular to the ambient electric field. We consider local sinusoidal perturbations of 5%–100%, as induced from discharge shock waves. We use a cylindrically symmetric particle-in-cell code to simulate the evolution of bidirectional streamers and compare the electron density, electric field, streamer velocity and electron energy of streamers in uniform air and in perturbed air. In all considered cases, the motion is driven along in decreasing air density and damped along increasing air density. Perturbations of at most 5%–10% change the velocity differences by up to approximately 40%. Perturbations perpendicular to the electric field additionally squeeze or branch streamers. Air variations can thus partly explain the difference of velocities and morphologies of streamer discharges. In cases with large perturbations, electrons gain energies of up to 30 keV compared to 100 eV in uniformly distributed air. For such perturbations parallel to the ambient electric field, we see the spontaneous initiation of a negative streamer; for perpendicular perturbations, x-rays with energies of up to 20 keV are emitted within 0.17 ns.

Keywords: streamers, air perturbations, x-rays

1. Introduction

Streamers, small, filamentary plasma channels of negative or positive polarity moving through air, form the early stages of lightning leaders [1–5] and of transient luminous events [6–13]. Their propagation mechanisms depend on their polarity: positive streamers propagating along electric field lines require an additional electron source, by background ionization [14, 15] or ionization through UV photons [16–20], to support their motion, whilst negative streamers move through the acceleration of electrons against the electric field lines out of the streamer head and the subsequent ionization of air molecules ahead facilitated by UV photoionization (e.g. see discussions in [17, 21]). In a recent work [21], we discovered that the emission of Bremsstrahlung photons by electrons accelerated in the streamer head and their photoionization also contribute to the propagation of streamers and their filaments in nitrogen–oxygen mixtures with low oxygen concentrations. For both polarities, we thus need three key ingredients for the inception and propagation of streamers: an initial source of free electrons with a sufficiently high charge density, an ambient electric field to accelerate electrons and an ambient gas medium ionizable by accelerated electrons and emitting new electrons to sustain the streamer propagation.

Luque *et al* [11] simulated the destabilization of a halo as well as the inception and propagation of sprite streamers between 55 and 85 km altitude from an exponentially increasing ambient electron density. Since sprite streamers extend over a range of several km, it is essential to take into account the decrease of the air density with altitude, which is an intrinsic feature of the Earth's atmosphere.

[3] Author to whom any correspondence should be addressed.

Further simulations of the formation and motion of sprite streamers [22–26] have all taken the altitude dependence of the air density into account. Opaits *et al* [27] investigated the development of streamer discharges in laboratory experiments mimicking sprite streamers on a smaller scale. They studied streamers in air density gradients along the discharge gap and discovered that streamers initiated in low air density regions and moving along increasing density, initially move faster and branch more easily than in uniform air.

Briels *et al* [28] have investigated the similarity laws of positive streamers in air and in nitrogen with a purity of approximately 99.9% in laboratory experiments. They altered the different ambient pressures between 0.013 to 1 bar, being equivalent to changing the density of ambient air molecules. They found that the minimal streamer diameter is inversely proportional to the pressure and that the streamer velocity changes with pressure. The similarity of streamers at different pressures is related to the mean free path length of electrons being inversely proportional to the ambient gas density. Since the rate of electrons colliding with air molecules depends on the mean free path and the energy gained through the available electric field, streamers in the same ratio of the ambient field and density behave similarly. This is known as Townsend's scaling.

Townsend's scaling relates streamer properties at ground pressure to pressures at higher altitudes [8, 29] and simulations have shown the similarity between streamers at ground pressure and sprite streamers [30]. The temporal and spatial scales of discharges, and the strength of the electric field, are inversely proportional to the neutral density. This arises from simple considerations of the mean free path for electrons [28, 30, 31]. Therefore, significant differences are to be expected in the case of perturbing the air density locally.

Some early discussions of density perturbations in connection with discharges are found in Marode *et al* [32], suggesting that streamers, before the formation of a hot conductive leader channel, induce a radial flow of neutral air molecules through thermal expansion, which reduces the air density by up to 50% and facilitates the electron motion and thus the spark breakdown. Similar conclusions were reached for positive streamers in a point-plane electrode geometry in the more recent simulations in [33, 34]. Orville [35] developed a return-stroke model based on experimental data for the temperature and electron density in a return stroke [36, 37] coupled with Gilmore's tables of thermodynamic properties [38]. He showed that the relative mass density in the hot return-stroke channel is decreased by a factor of four and that the number density of nitrogen molecules is reduced up to one order of magnitude within a 10 m section and within 30 μs after a model-return stroke. Similarly, Eichwald *et al* [39, 40] found the gas density was reduced $\simeq$50% in the vicinity of spark discharges. More recent simulations show that, in the vicinity of a positive polarity point electrode, the shock wave induced by a streamer will heat the air to 2000 K, which is equivalent to a decrease of the air density of up to 85% [41]. Additionally, experiments have shown that the pressure difference induced by spark discharge shock waves can reach values of up to ten times the ambient air pressure [42]. In the vicinity of lightning leaders, this pressure difference is sufficiently high to perturb the air density by up to a factor of 100% [43].

Besides radial perturbations induced by shock waves of proximate streamer and leader discharges, heating processes [44–46] can perturb the spatial distribution of air molecules locally in a vertical extension. Large-scale perturbations with large pressure gradients and, hence, air density gradients can also be initiated by civil transport aircraft, high-speed air vehicles or by the wind flow around (sharp) objects [47–52]. Little is known about the effect of such air perturbations on streamer properties. Here, we study the effects of perturbations on the morphology and velocity of bipolar streamers at ground pressure. We consider uniform air density and compare with results in perturbed air with the same number of neutral particles.

In section 2, we describe our model. We define the computational domain as well as the initial conditions and describe the implementation of the air perturbations. In section 3, we present results for different density variations vertically and horizontally relative to the ambient electric field lines. We compare the electron density, the electric field and the streamer velocities. Finally, we present our conclusions in section 4.

2. Modeling

2.1. Set-up of the model

To investigate the motion and development of streamers, we trace electrons through air using a 2.5D cylindrically symmetric particle Monte Carlo code with two spatial coordinates (r, z) and with three velocity coordinates (v_r, v_θ, v_z). As in [21, 53], we initiate a Gaussian electron–ion patch with a peak density of $n_{e,0} = 10^{20}$ m^{-3} and a width of $\ell = 0.2$ mm centered at $z_0 = 7$ mm. The size of the simulation domain is $L_r = 1.25$ mm in r direction and $L_z = 14$ mm in the z direction. The ambient field E_{amb} is 1.5 times the classical breakdown field in uniform air, $E_k \equiv 3.2$ MVm^{-1}, at standard temperature (300 K) and pressure (1 bar) and is pointing from the upper to the lower boundary; after every time step we solve the Poisson equation on a mesh with 150 grid points in r and with 1200 grid points in z direction. We have chosen $E_{\mathrm{amb}} = 1.5E_k$ that is common in the literature and corresponds to a relatively weak field, allowing the initiation of a streamer from a single electron. This field strength and higher fields can be found in sprite streamers [30, 54] or laboratory discharges [18]. At the boundaries ($z = 0, L_z$), we use the Dirichlet boundary conditions $\phi(r, 0) = 0$ and $\phi(r, L_z) = E_{\mathrm{amb}} \cdot L_z$, and at ($r = 0, Lr$) we use the Neumann boundary conditions and fix the electric field strength to zero. Details about the collisions of electrons with air molecules and their numerical implementation can be found in [21, 55].

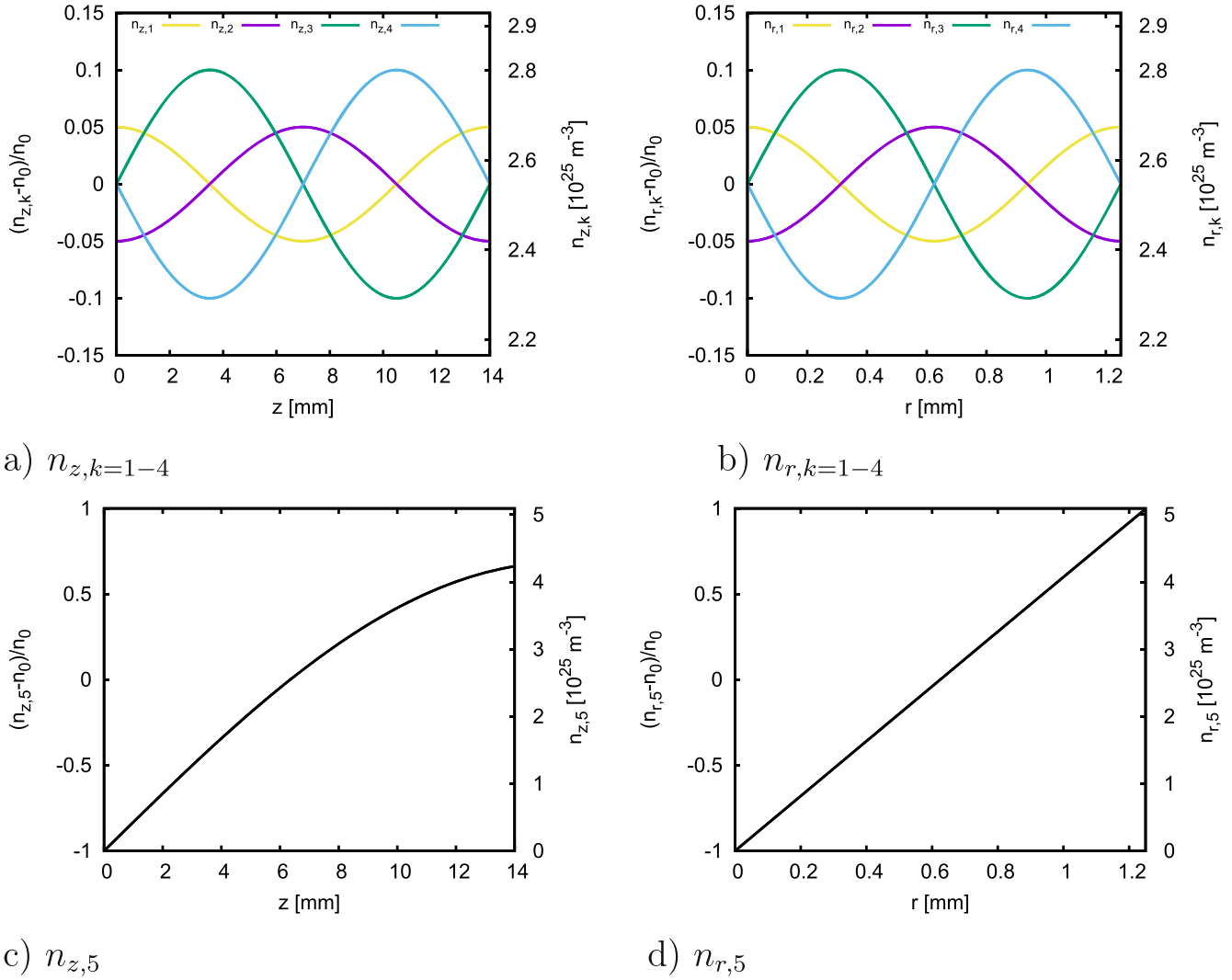

Figure 1. The air densities (1)–(4) as a function of (a), (c) z and as a function of (b), (d) r. The densities are expressed in terms of the relative difference $(n_{z/r,k} - n_0)/n_0$ with $n_0 \approx 2.55 \times 10^{25}$ m^{-3}; the right y-axis shows n.

For the particle management, i.e. merging and splitting superelectrons, we use the same scheme as elaborated in [21, 55] and references therein.

2.2. Density perturbations

One of the key ingredients governing the motion of streamers is the composition and the density of ambient gas. The mean free path Λ of electrons between two collisions with air molecules is $\Lambda = (n\sigma_t)^{-1}$, where σ_t is the total cross section of electrons scattering off air molecules and n is the air density. Equivalently, the motion and energy of electrons in a gas is governed by the reduced electric field E/n. Since the electron's mean free path and the reduced electric field depend on n, the spatial distribution of n is crucial to understand the motion of electrons in air.

To investigate the effect of perturbed air on the streamer dynamics, we simulate the motion of streamers in uniformly distributed air density $n_0 \equiv 2.55 \times 10^{25}$ m^{-3} and in sinusoidal densities $n(r, z)$ depicted in figures 1(a) and (b):

$$n_{z,k}(z) = a_k \cdot \sin(b_k \cdot z + c_k) + n_0, \quad (1)$$

$$n_{r,k}(r) = a_k \cdot \sin(b_k \cdot r + c_k) + n_0, k \in \{1, \ldots, 4\}, \quad (2)$$

with a, b and c as tabulated in table 1. Additionally, we investigate the properties of streamers in air with the spatial distributions

Table 1. The input parameters for densities (1) and (2).

	a_k [10^{23} m^{-3}]	b_k [m^{-1}]	c_k
$n_{z,1}$	12.74	−448.80	$1/2\ \pi$
$n_{z,2}$	12.74	−448.80	$3/2\ \pi$
$n_{z,3}$	25.47	−448.80	π
$n_{z,4}$	25.47	−448.80	$2\ \pi$
$n_{r,1}$	12.74	−5026.55	$1/2\ \pi$
$n_{r,2}$	12.74	−5026.55	$3/2\ \pi$
$n_{r,3}$	25.47	−5026.55	π
$n_{r,4}$	25.47	−5026.55	$2\ \pi$

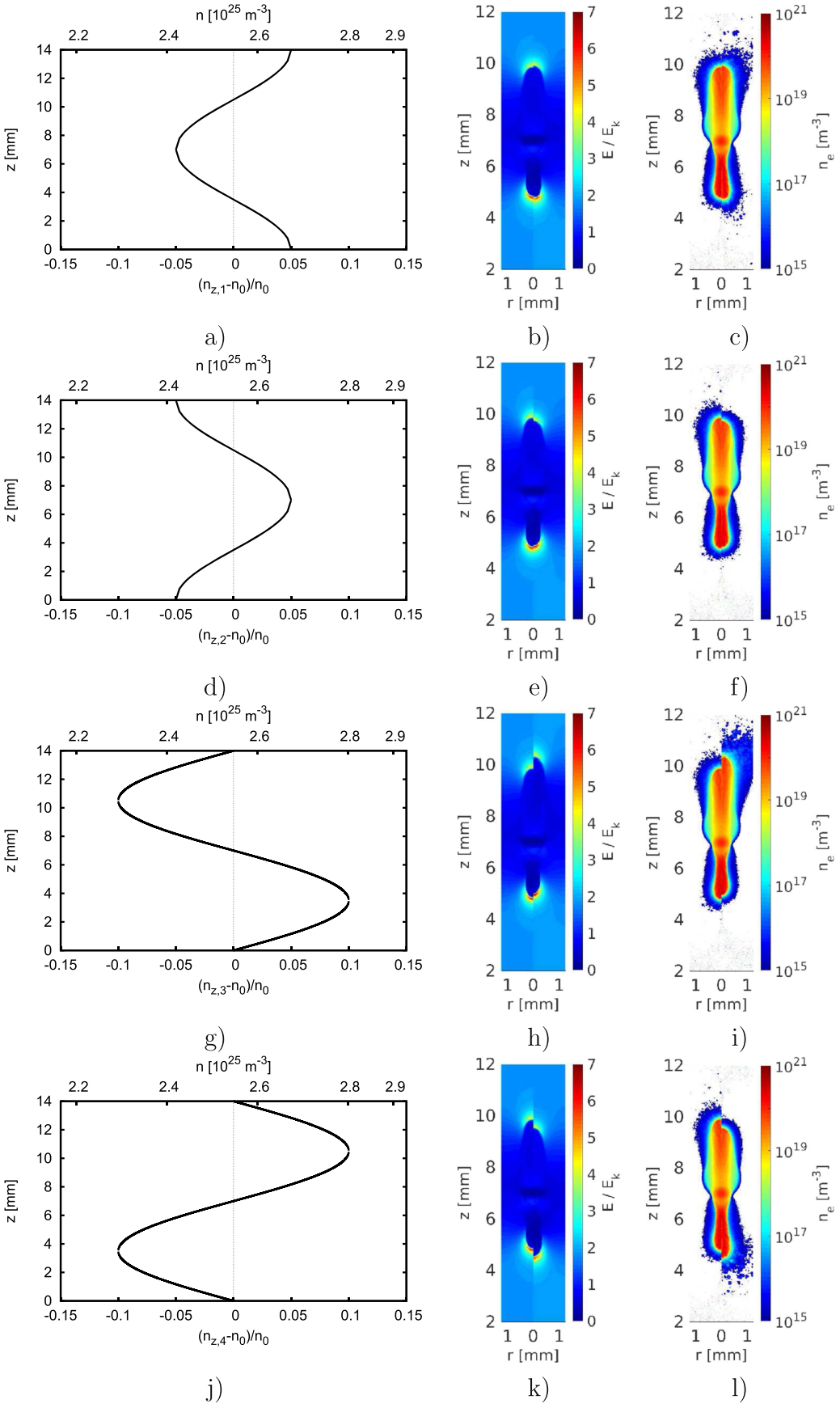

Figure 2. The electric field (second column) and the electron density (third column) of streamers after 2.59 ns in different air densities. The left half of the field and density shows results in uniform air n_0 and the right half in perturbed air $n_{z,1-4}$ (first column, equation (1)).

Table 2. The mean velocities $v^{\pm}$ and normalized mean velocities $(v/v_0)^{\pm}$ of the positive and negative streamer front between 0.54 ns and 2.59 ns in different air densities.

	v^+ [10^6 m s^{-1}]	v^- [10^6 m s^{-1}]	$(v/v_0)^+$	$(v/v_0)^-$
$n_{z,1}$	1.01	1.37	1.11	1.18
$n_{z,2}$	0.91	1.15	1.00	0.99
$n_{z,3}$	0.81	1.59	0.89	1.37
$n_{z,4}$	1.13	1.13	1.24	0.97
$n_{r,1}$	0.51	0.70	0.56	0.60
$n_{r,2}$	1.51	1.60	1.66	1.38
$n_{r,3}$	0.84	1.06	0.92	0.91
$n_{r,4}$	0.88	1.09	0.97	0.94

$$n_{z,5}(z) = 4.39 \times 10^{25} \cdot \sin(z/\zeta)\ \mathrm{m}^{-3}, \tag{3}$$

$$n_{r,5}(r) = 4.08 \times 10^{26} \cdot \sin(r/\zeta)\ \mathrm{m}^{-3} \tag{4}$$

with $\zeta = 1$ cm shown in figures 1(c) and (d). We have chosen sinusoidal functions since the air density is modulated as a sinusoidal wave after the appearance of a shock wave. With these density functions we simulate the effects of air density perturbations after shock waves and thermal expansion induced by streamer or spark discharges [32, 41, 42, 56] or in the vicinity of high-speed air flows creating large pressure gradients and subsequently large air gradients [49, 50, 52]. We refer to (1) and (3) with their gradients along the z-axis as perturbations parallel to the ambient electric field; likewise we refer to (2) and (4) as perturbations perpendicular to the ambient field. The functional shape is chosen such that there are different regions with different numbers of air molecules. We note here that, in reality, in long discharges not only one, but multiple streamers occur [58]. Although there are rarely models describing the interaction of several streamers amongst each other [59–61], it is thus not unlikely to assume that a couple of streamers perturb ambient air whilst others travel in such perturbed air region. Other than that, the actual shape of the chosen functions is not important for our conclusions.

3. Results

Under the influence of the ambient electric field, the initial electron patch develops into a double-headed streamer; the negative front propagates upwards, the positive one downwards. Figure 2 shows the electron density and the electric field for air density (1); figure 7 shows the electron density and the electric field for air density (2). In the panels showing the electric field and the electron density, the left half shows results in uniformly distributed air n_0 whereas the right half shows results for perturbed air.

3.1. Perturbations parallel to the ambient field lines

We first look into the evolution of bidirectional streamers for heated or compressed air parallel to the ambient electric field; the air density profile of these scenarios is described by (1) or (3). The third column of figure 2 compares the electron density in uniformly distributed air (left half of each panel) with the electron density in perturbed air (1) (right half); the second column shows the corresponding electric fields. Panels (a)–(f) of figure 2 demonstrate that streamer inception at the position of maximal density elongation ($n_{z,1}$ and $n_{z,2}$) does not alter the shape and the velocity of a streamer significantly since the number density of air molecules quickly reaches the density n_0 corresponding to uniform air. If the streamer is initiated in reduced air density ($n_{z,1}$), the streamer fronts have advanced slightly further than in non-perturbed air; contrarily, if the streamer is initiated in higher air density ($n_{z,2}$), the streamer fronts are slightly damped.

The effect on the shape and on the velocity is much more significant if the streamer inception takes place at the position of maximal and minimal slope of the air density ($n_{z,3}$ and $n_{z,4}$), which leads to a rapid deviation from the air density n_0 of uniform air. Since the densities grow and fall to different sides, both fronts behave contrarily. In $n_{z,3}$ the negative front is faster than in n_0 whilst the positive front is slower, vice versa for $n_{z,4}$. Panels (i) and (l) demonstrate that ionization is pronounced ahead of the streamer in regions with high air density independent of the polarity of the streamer front; accordingly, for low density regions, the streamer front is thinner.

Table 2 shows the mean streamer velocities

$$v^{\pm} := \frac{z^{\pm}(t_1) - z^{\pm}(t_0)}{t_1 - t_0}, \tag{5}$$

where $z^{\pm}(t_{0,1})$ is the position of maximum electric field strength on the positive or negative streamer head after $t_0 = 0.54$ ns and $t_1 = 2.59$ ns, as well as the normalized mean velocities $(v/v_0)^{\pm}$. The mean velocities in all cases are in the order of 10^6 m s^{-1}. In all our simulations, negative fronts are faster than positive fronts, which is consistent with previous work [62, 64]. However, this is only the case for the very first time steps of the streamer evolution; at later stages, the positive front moves faster than the negative front [62]. Indeed, experiments performed by [65] and other modelling efforts [30] have shown that positive fronts move faster than negative ones because of their rather high peak field. However, since the motion of streamers in our simulations is governed by the air density profile, the following results can be extended very easily to faster positive fronts irrespective of the relative speed between the negative and positive front. In density $n_{z,1}$ both streamer fronts move approximately as fast as in constant air density n_0; in $n_{z,2}$ the negative streamer front is ≈20%, the positive one ≈10% slower than in n_0. In $n_{z,3}$ and in $n_{z,4}$ the streamer fronts moving within the region of increasing air density move slower whereas the fronts within decreasing air density move faster compared to the motion of streamer fronts in constant air density. This is in agreement with observations made by Opaits *et al* [27] that (positive) streamers move faster in air densities small compared to n_0.

Figure 3(a) shows the electron density in $n_{z,3}$ (left half) and in $n_{z,4}$ (right half) after 2.59 ns; in the right half we mirrored the electron density plot at $z = 7$ mm compared to the density plot in the right half of figure 2(l). Hence, the

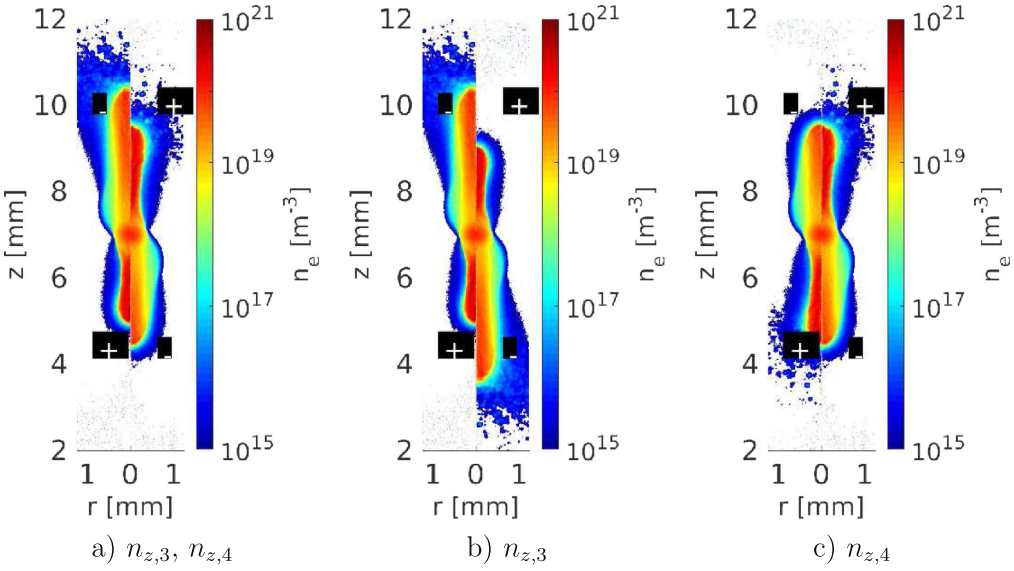

Figure 3. (a) The electron density in $n_{z,3}$ (left half) and in $n_{z,4}$ (right half) after 2.59 ns. In the right half, the density was mirrored at $z = 7$ mm compared to the right half of figure 2(l). (b), (c) The electron density (left half) and the same electron density mirrored at $z = 7$ mm (right half) after 2.59 ns in $n_{z,3}$ (b) and in $n_{z,4}$ (c). The black boxes indicate the polarity of the streamer.

spatial distribution of air molecules in both halves looks like $n_{z,3}$, and we can explicitly compare positive and negative streamers in the same air density profile. The negative streamer front moves faster than the positive one because of the different propagation mechanisms [62–64]; the negative streamer front moves through the motion of electrons against the electric field and the subsequent ionization in front of the streamer head facilitated by photoionization [17], whereas photoionization ahead of the streamer head is essential for the motion of the positive front. Given the mean velocities in table 2, the negative front moves approximately 40% faster than the positive one in the same density profile.

Panels (b) and (c) show the electron density (left half) and the mirrored electron density (right half) in air densities $n_{z,3}$ (b) and $n_{z,4}$ (c) giving us the opportunity to immediately compare the different elongations of the negative and the positive front. It shows that in $n_{z,3}$ the negative front moves almost twice as fast as the positive one; in $n_{z,4}$ both streamer fronts move equally fast. Since the air density decreases with increasing z for $n_{z,3}$, i.e. against the electric field, the reduced electric field increases in the direction of electron drift and the electron energy is enhanced. Since the air density increases downwards, the reduced electric field in that region decreases and the electron motion is damped. In $n_{z,4}$ the opposite takes place: the air density increases against the electric field, i.e. in the direction of electron drift, and decreases at the positive tip, i.e. along the electric field. Hence, electron motion at the negative front is damped whereas the electron energy in the vicinity of the positive front is favored, such that both fronts move equally fast. Controlling the air density profile parallel to the ambient electric field, is thus a mean to align the mean velocities of negative and positive streamers.

3.2. Spontaneous initiation of a negative streamer

Figure 4 compares the electron density of a streamer initiated at $z = 7$ mm in uniform air density (left half of each panel) with the electron density of a streamer in air density (3). Equation (3) describes the spatial distribution after a shock wave where the majority of air molecules is shifted to the upper boundary. After 1.05 ns the motion of both streamer fronts is suppressed; at the negative tip the air density is increased, hence the reduced electric field E/n is decreased and the electron motion is damped. At the positive front, the air density is decreased much more than for $n_{z,4}$. Although the reduced electric field is thus increased and electrons gain more energy than in uniform air, the ionization coefficient is decreased for very small air densities and so is the probability of photoionization.

The motion of the negative front in air density (3) is damped during the whole simulation. Whilst the mean velocity of the negative streamer between 1.05 ns (a) and 2.24 ns (d) in uniformly distributed air is 1.09×10^6 m s^{-1}, the average velocity is 0.66×10^6 m s^{-1} in perturbed air density, hence a factor of approximately 1.6 slower.

The propagation of the positive streamer front is, however, not damped during the whole simulation. Figure 5 zooms in on the electron density into the region $z = 0.5$–2.5 mm between 1.34 ns and 1.71 ns; here the air density varies from $0.1n_0$ at 0.5 mm to $0.42n_0$ at 2.5 mm. We observe that a small electron inhomogeneity is produced by UV photoionization at approximately 0.5 mm (panel (a)). It first turns into an electron avalanche (panel (b)) and then further into a negative streamer (panels (c) and (d)). Panels (e) and (f) show the electric field after the same time steps as in panels (c) and (d). They show the typical field pattern of a streamer with enhanced field strengths at the channel tips and vanishing field in the body. Here we also note that there are

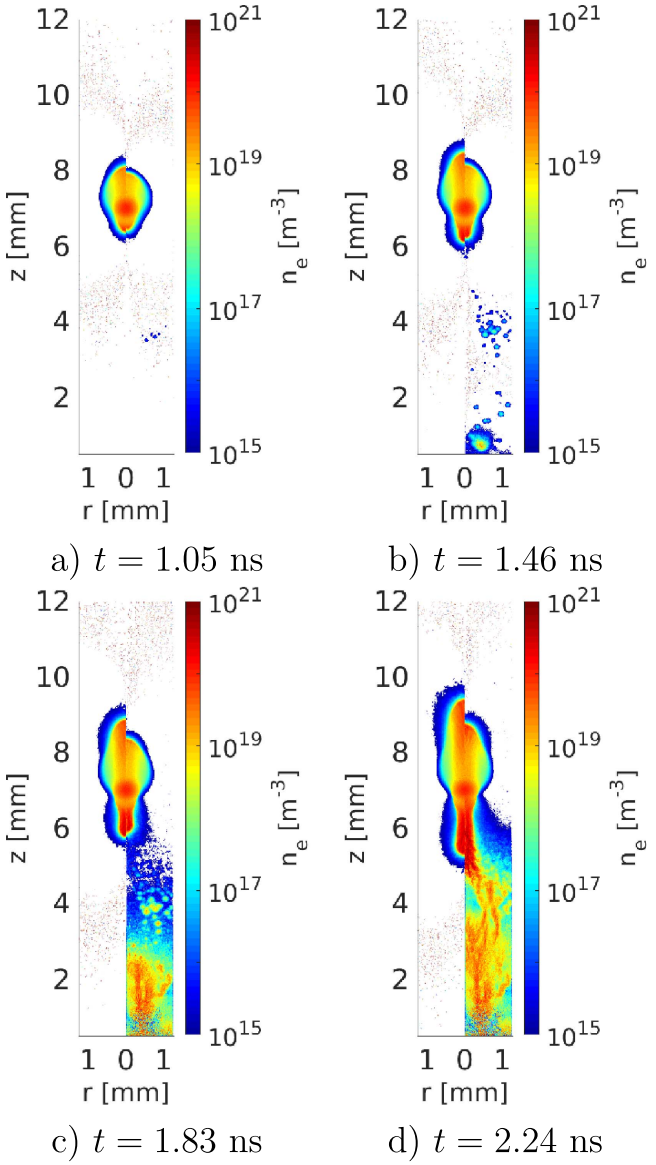

Figure 4. The electron density in uniform air (left half in each panel) and in air distributed according to density (3) (right half).

several local electron patches below 2.5 mm, supporting the initiation of a negative streamer. Since we use a 2.5 dimensional Monte Carlo code, the patches illustrated in figure 5 actually have a cylindrical shape. We note that fully three-dimensional simulations would be desirable to confirm our observation of the spontaneous inception and motion of a negative streamer. However, although we cannot exclude that this is a numerical artifact, our microphysical interpretation of the observed phenomena, i.e. the production of local electron patches through photoionization and the further multiplication of the electron number, is independent of the dimensionality of the used Monte Carlo code. Subsequently, the positive front of the original streamer and the newly formed negative streamer encounter and accelerate each other [53, 66] such that the positive front finally moves faster than in uniformly distributed air. However, we here strongly emphasize that the production of such an electron inhomogeneity and the formation of a negative streamer is a rare event. Fortunately, we were able to capture such an event, but we do not expect this pattern to occur in all simulations with the same air density profile and ambient electric field.

Figure 6 shows the electron energy distributions in non-perturbed (solid) and in perturbed air $n_{z,5}$ (dashed) after 1.83 ns. The solid line shows a typical streamer-like energy distribution with energies of at most 100 eV [55]. In contrast, the dashed line shows an energy distribution with energies of up to 3 keV. As stated by Cooray *et al* [67], the collision of two encountering streamers could eventually lead to fields sufficiently high to produce electrons with energies of several hundreds of keV. In contrast, recent work [53, 66] has shown that the collision of two streamers alone cannot produce a sufficient number of runaway electrons. However, here we observe the production of a significant number of electrons above 500 eV between two colliding streamers in perturbed air which could eventually lead to the production of x-rays with energies of a few keV.

3.3. Perturbations perpendicular to the electric field

For perturbations perpendicular to the ambient electric field, for example induced by shock waves, e.g. induced by bypassing lightning strikes or neighboring streamers [68], the spatial distribution of air molecules can be approximated by equation (2). Figure 7 shows the electron density and the electric field after 2.59 ns. The first row shows the electron density in the case that the air density is 5% higher than n_0 at $r = 0$ and decreases for increasing r; the second row shows the electron density in case the air density is 5% smaller than n_0 at $r = 0$ and increasing for increasing r. Since the streamer develops close to $r = 0$, its evolution is damped in the first case and driven in the second case. This is the same effect as we have observed in figure 2 for variations in the z direction. Table 2 shows that, in the first case, both streamer fronts are slower by approximately 40% whereas they are faster by a factor of up to 66% in the second case. The third and the fourth rows show the electron density and electric field if the air density equals n_0 in the vicinity of streamer inception and then starts increasing (third row) or decreasing (fourth row) for increasing r. In these cases, the streamer fronts are equally fast as streamers in uniform air, see table 2. In the third row we observe a slight streamer quenching and the emergence of another electron avalanche in the low air density region, which is comparable to the emergence of the electron avalanche in figure 4(b). The fourth row shows that, if the air density first decreases, the streamer follows the air density resulting in turning away from the symmetry axis. Additionally, the reduced electric field is enhanced due to the reduced air density. Since we use a Monte Carlo code with cylindrical symmetry, any deflection from the symmetry axis resembles branching. This resembles the effect of a magnetic field influencing the streamer motion. In strong magnetic fields between 1 T and 10 T, streamers at standard temperature and pressure have been observed to bend and branch compared to streamers in vanishing magnetic fields [69, 70]. This is the case for magnetic fields sufficiently strong such that the gyration frequency of electrons exceeds the collision frequency of electrons scattering off air molecules (see e.g.

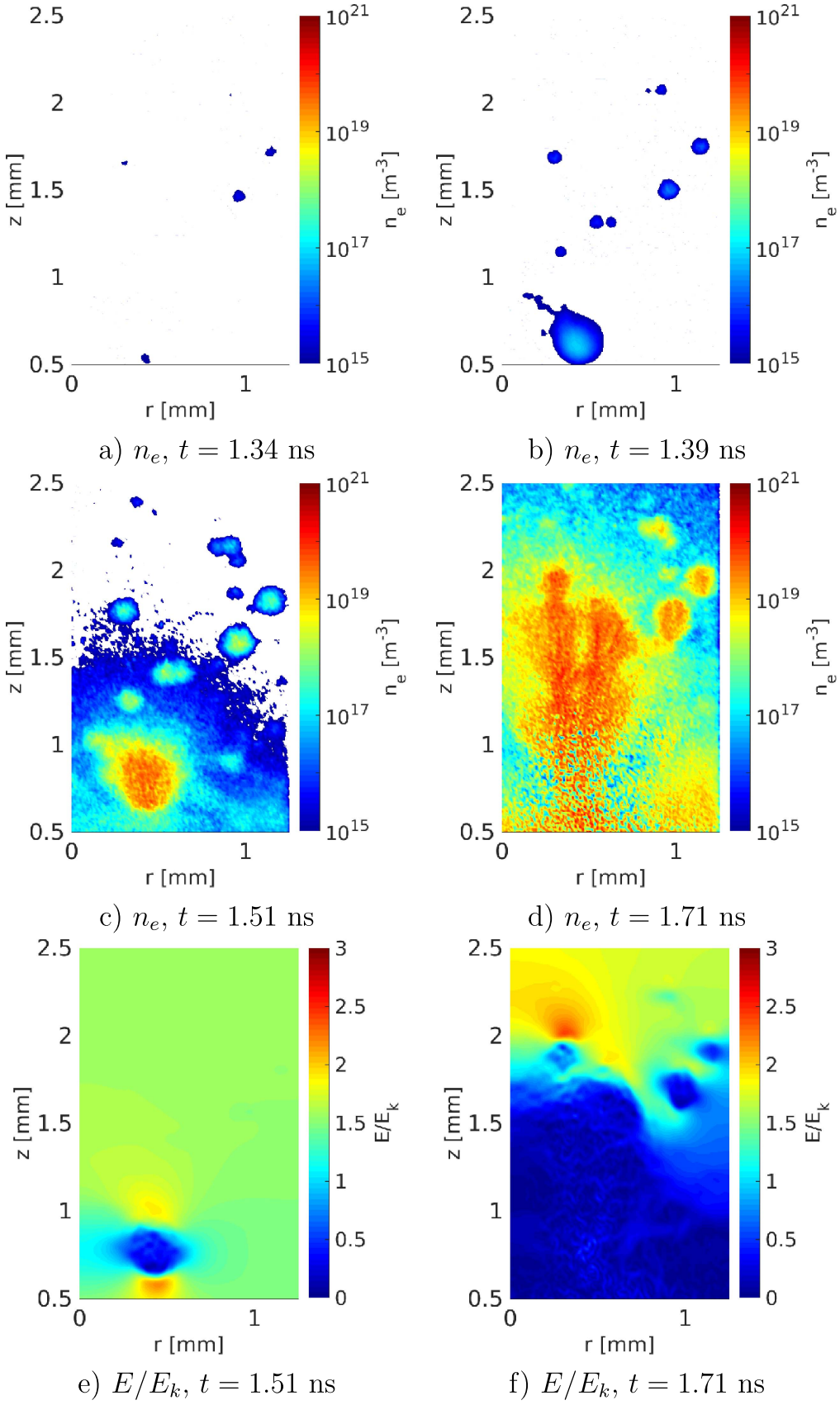

Figure 5. The electron density (a)–(d) in air density (3) zoomed in to $z = 0.5$–2.5 mm after different time steps. (e), (f) The electric field for the same time steps as in (c) and (d).

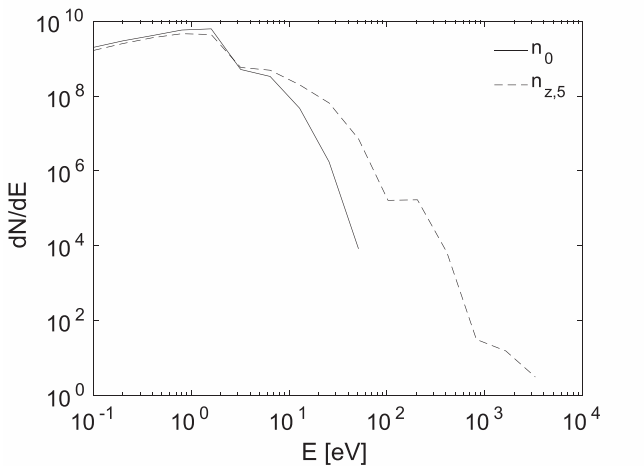

Figure 6. The electron energy distribution in air densities n_0 (solid) and $n_{z,5}$ (dashed) after 1.83 ns.

[31, 71] for discussions of the gyration and collision frequency). Additionally, we see a widening of the electron density in the r direction.

3.4. Occurrence of Bremsstrahlung photons in perpendicularly perturbed air

Figure 8 compares the electron density in uniform air (left half) and in air density (4) (right half) after different time steps. The shape of the air density (4) describes the spatial distribution of air molecules after a shock wave where the majority of the air molecules is located at the exterior of the simulation domain. Spherical and cylindrical shock waves associated with lightning leader propagation create large overpressures such that the air density in its vicinity is reduced by up to 100% [42, 43]. Figure 8 shows that in the latter case the electron density in the direction of the negative front grows much faster than in air density n_0. Since for the second case the air density is smaller in the vicinity of the symmetry axis, the the drift speed of electrons upwards is larger and the ionization of air molecules ahead of the initial electron patch are facilitated.

The positive front is less pronounced than the negative front since the decreased air density close to the symmetry axis reduces the probability of photoionization events.

Figure 9 compares the energy distributions of electrons in uniform and in perturbed air and shows the energy distribution of Bremsstrahlung photons in perturbed air after 0.17 ns. Whereas in non-perturbed air electrons have reached energies of up to only 100 eV, electrons gain energies of up to 20 keV in perturbed air. As a consequence, high-energy electrons produce Bremsstrahlung photons with energies of up to 20 keV.

Figure 10 shows the position of Bremsstrahlung production; every single point in that figure represents one Bremsstrahlung producing event. Since the majority of air molecules is moved away from the symmetry axis, no Bremsstrahlung photons are produced in its vicinity. Instead, electrons are first accelerated in the low air density region with its high reduced electric field, subsequently reach the high density region and finally create Bremsstrahlung photons by scattering at air molecules.

4. Conclusions and outlook

We have observed how the properties of negative and positive streamers alter in perturbed air in relation to shock waves or heating.

Variations of the spatial distribution of air parallel to the ambient electric field of about 5%–10% damp or drive the streamer motion along increasing or decreasing air density. The mean streamer velocities differ up to approximately 40% from the mean velocities of streamers in uniformly distributed air. Thus, the velocity of streamer discharges significantly depends on the spatial distribution of ambient air.

For strong perturbations where the majority of air molecules is located close to the upper boundary, we have observed the spontaneous emergence of an additional negative streamer in the low density region moving towards the anode and finally colliding with the positive front of the original streamer. Whereas the collision of streamers in uniform air is unlikely to produce runaway electrons and, subsequently, x-rays, the collision of two streamers in perturbed air enhances the electron energy and yields energies of at least 3 keV. This gives a possible scenario where the encounter of streamers can explain the emission of x-rays.

Perturbations perpendicular to the ambient electric field have three different implications. First, if the density close to the streamer inception is enhanced or reduced relative to constant air density, the streamer motion is damped or driven parallel to the ambient field by a factor of up to 60% relative to the motion of streamers in uniform air. Similar to perturbations parallel to the electric field lines, we thus conclude that the velocity of lightning leaders is affected by radial perturbations.

Second, if the value of the air density in the vicinity of streamer inception is as large as for unperturbed air and subsequently starts altering, streamer quenching or branching occurs. Hence, in radial perturbations not only the velocity, but also the morphology of, streamers and leaders depend on the distinct distribution of air molecules.

Third, for perturbations where the presence of air molecules is negligible in the vicinity of the initial electron–ion patch, electrons are accelerated to energies of up to approximately 20 keV, subsequently creating x-rays with comparable energies within 0.17 ns. Hence, strong radial perturbations explain the emission of x-rays from streamer discharges; comparably the emission of gamma-rays from lightning leaders is facilitated in perturbed air.

Since air flow in the vicinity of high-speed air vehicles can include shock waves and subsequently high pressure gradients [49, 50, 52], we believe that discharge properties are altered in the proximity of such air vehicles. Depending on the discharge polarity and the degree of perturbation, various

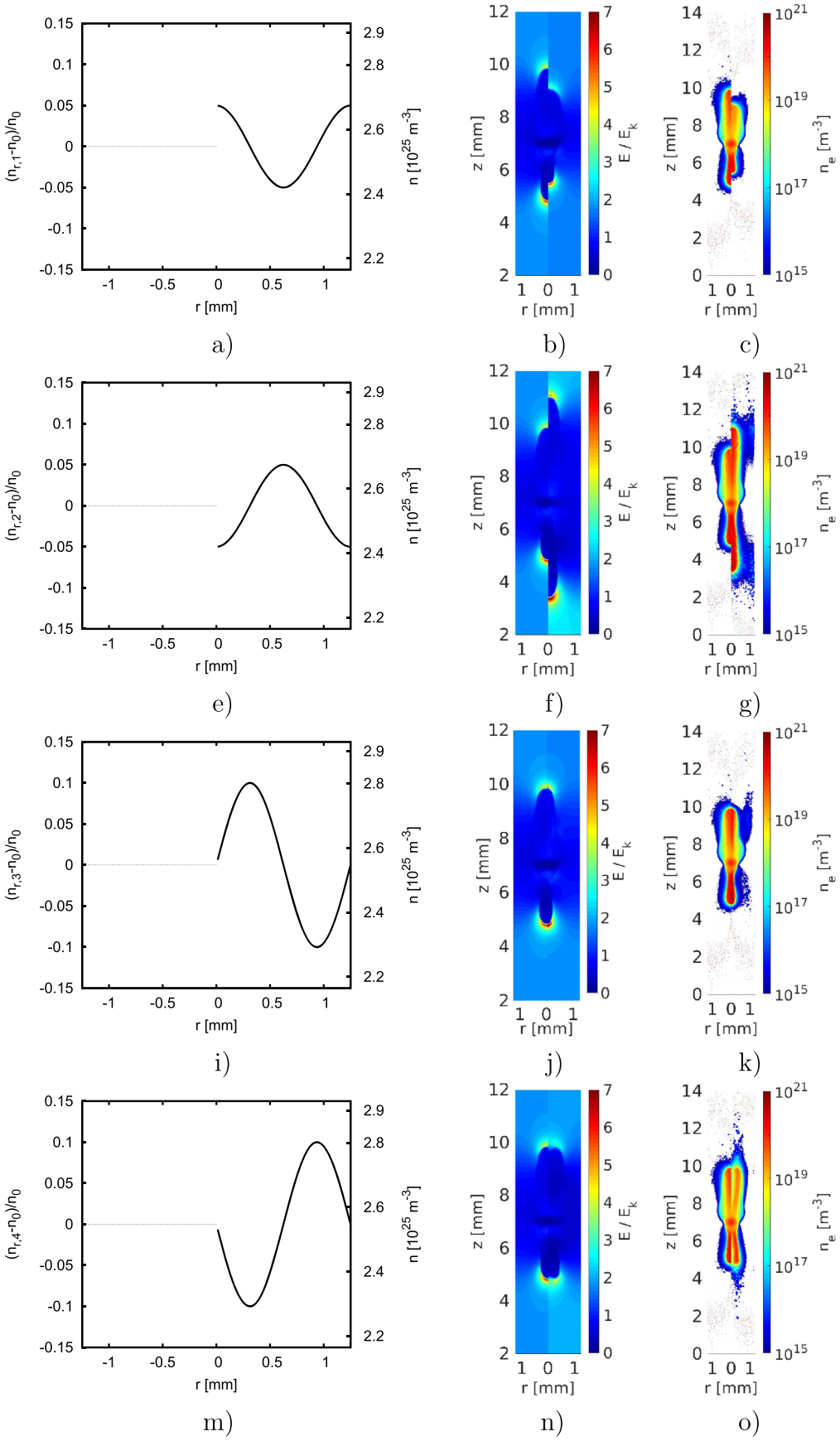

Figure 7. The electric field (second column) and the electron density (third column) of streamers after 2.59 ns in different air densities. The left half of the field and density shows results in uniform air n_0 and the right half in perturbed air $n_{r,1-4}$ (first column, equation (2)).

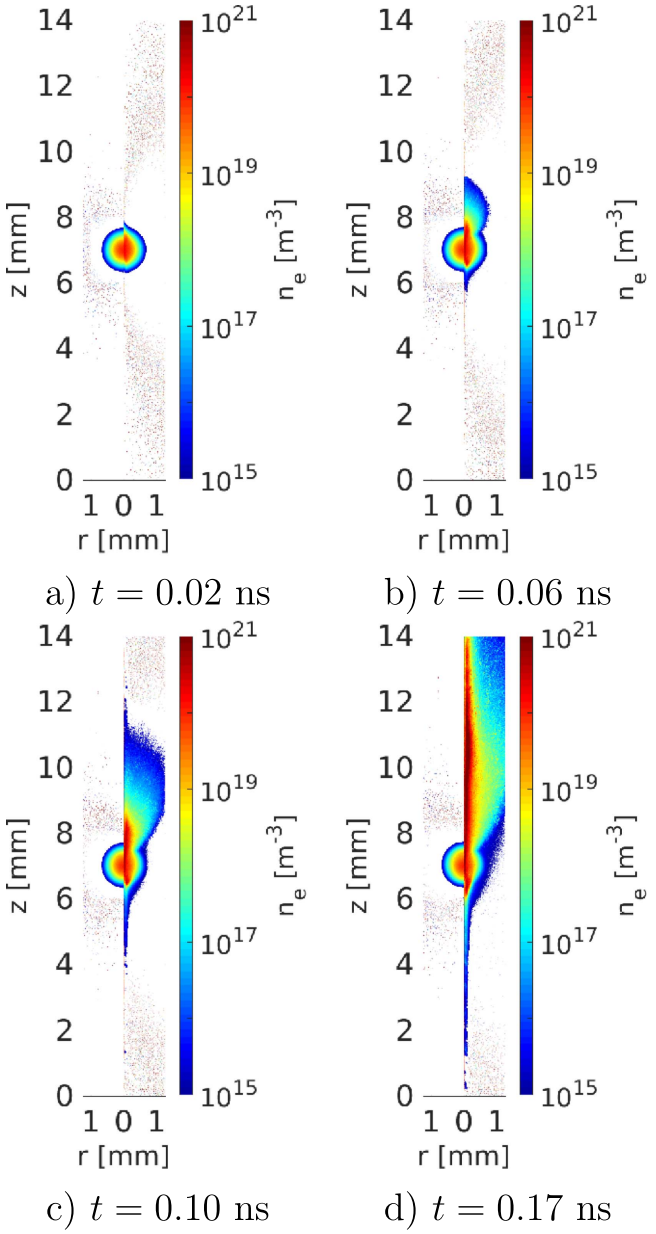

Figure 8. The electron density in uniformly distributed air (left half in each panel) and in air distributed according to density (4) (right half).

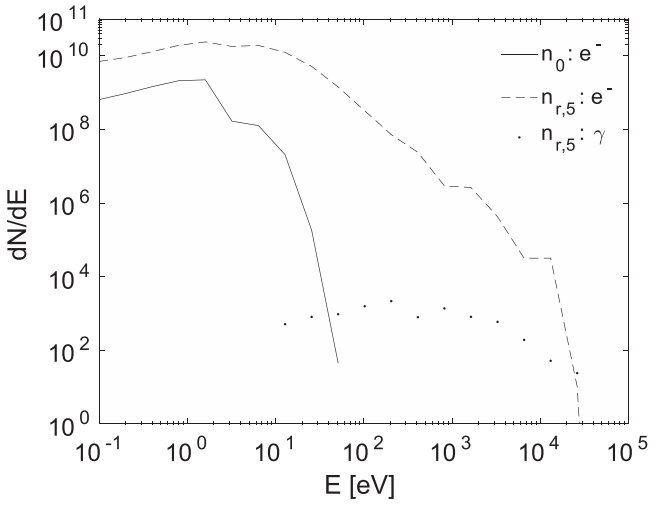

Figure 9. The energy distribution of electrons in uniform air density n_0 (solid) and in $n_{r,5}$ (dashed) and of photons in $n_{r,5}$ (dotted) after 0.17 ns.

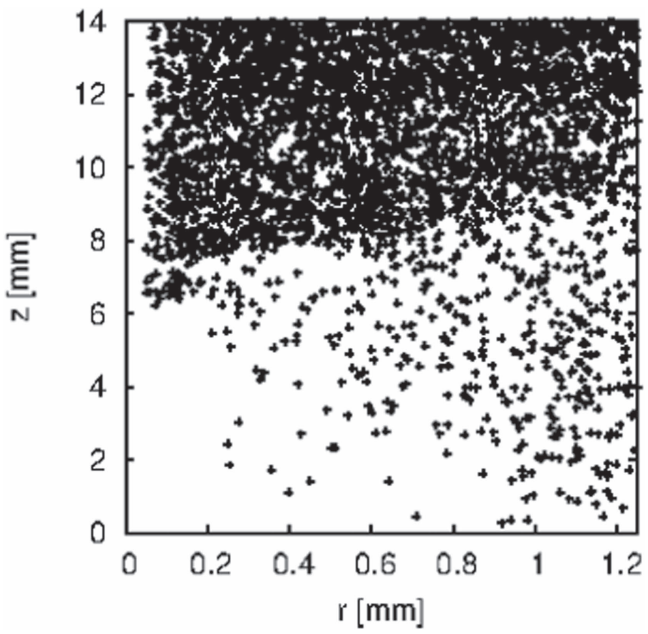

Figure 10. The position of Bremsstrahlung production time-integrated until 0.17 ns in the simulation domain. Every dot represents the creation of one Bremsstrahlung photon; for better visibility the figure is not true to scale.

scenarios are imaginable: for negative discharges and moderate shock waves, because the ambient air is perturbed with a level of only a few tens of %, we expect the discharge motion to be facilitated and eventually reach the aircraft more easily. In contrast, for positive polarity and shock waves with large air perturbations, we speculate that the discharge will die before it reaches the air vehicle. However, large-scale discharges like lightning leaders have different motion mechanisms than streamers (see e.g. a discussion in [4]); thus we emphasize that our findings can only serve as a first approximation of the discharge motion in air perturbations produced by high-speed air vehicles. Further simulations need to be performed to understand discharge properties close to moving structures including air turbulence.

To the best of our knowledge, there have not been many experiments dealing with the streamer properties of laboratory discharges in perturbed air. Mimicking sprites on a laboratory scale, Opaits *et al* [27] studied streamers in air density gradients parallel to the discharge gap, qualitatively agreeing with our results. Beyond that, there have been papers investigating the influence of wind flow on corona discharges [72, 73] or partial discharges [74]. However, these papers focus on macroscopic properties such as the corona onset voltage or current. Additionally, in these experiments not only is the spatial distribution of air molecules affected, but also the distribution of space charges. They do not investigate

microscopic streamer properties or the connection between air flow and x-ray emission.

We propose here to perform an experiment involving a shock tube (see e.g. [75, 76] for a discussion of the set-up and comparisons with numerical models). The shock tube is divided into a driver and driven section by a membrane. Small explosives in the vicinity of the membrane rupture it and create shock waves locally perturbing the spatial distribution of air molecules. Such a set-up allows placing two electrodes close to or in the shock tube; depending on the angle between the membrane and the electrodes and depending on the strength of the shock wave, one can investigate situations as they are set up in our simulations. Installing a camera system in the proximity of the discharge site then allows us to study the morphology and velocities of streamers. Additionally, we suggest installing x-ray detectors to study the effect of air perturbations on the production of x-rays.

Acknowledgments

The research leading to these results has received funding from the People Programme (Marie Curie Actions) of the European Union's Seventh Framework Programme (FP7/2007-2013) under REA grant agreement no. 609405 (COFUNDPostdocDTU).

ORCID iDs

C Köhn https://orcid.org/0000-0002-7101-5889
O Chanrion https://orcid.org/0000-0002-4484-4104
L P Babich https://orcid.org/0000-0003-1682-324X
T Neubert https://orcid.org/0000-0001-7851-7788

References

[1] Raizer Y P 1991 *Gas Discharge Physics* (Berlin: Springer)
[2] Raizer Y P, Milikh G M, Shneider M N and Novakovski S V 1998 *J. Phys. D: Appl. Phys.* **31** 3255–64
[3] Moss G D 2006 *J. Geophys. Res.* **111** A02307
[4] da Silva C L and Pasko V P 2013 *J. Geophys. Res.* **118** 561–90
[5] Montanyà J, van der Velde O and Williams E R 2015 *Sci. Rep.* **5** 15180
[6] Neubert T 2003 *Science* **300** 741–9
[7] Cummer S A, Jaugey N, Li J, Lyons W A, Nelson T E and Gerken E A 2006 *Geophys. Res. Lett.* **33** L04104
[8] Pasko V P 2007 *Plasma Sources Sci. Technol.* **16** S13–29
[9] Ebert U and Sentman D D 2008 *J. Phys. D: Appl. Phys.* **41** 23
[10] Pasko V P 2008 *Plasma Phys. Control. Fusion* **50** 124050
[11] Luque A and Ebert U 2009 *Nature Geosci.* **2** 757–60
[12] Celestin S and Pasko V P 2011 *J. Geophys. Res.* **116** A03315
[13] Qin J, Celestin S and Pasko V P 2012 *Geophys. Res. Lett.* **39** L05810
[14] Pancheshnyi S 2005 *Plasma Sources Sci. Technol.* **14** 645–53
[15] Nijdam S, Wormeester G, van Veldhuizen E M and Ebert U 2011 *J. Phys. D: Appl. Phys.* **44** 455201
[16] Zheleznyak M B, Mnatsakanian A K and Sizykh S V 1982 *High Temp.* **20** 357–62
[17] Luque A, Ebert U, Montijn C and Hundsdorfer W 2007 *Appl. Phys. Lett.* **90** 081501
[18] Bourdon A, Pasko V P, Liu N Y, Celestin S, Segur P and Marode E 2007 *Plasma Sources Sci. Tech.* **16** 656–78
[19] Wormeester G, Pancheschnyi S, Luque A, Nijdam S and Ebert U 2010 *J. Phys. D: Appl. Phys.* **43** 505201
[20] Xiong Z and Kushner M J 2014 *Plasma Sources Sci. Technol.* **23** 065041
[21] Köhn C, Chanrion O and Neubert T 2017 *Plasma Sources Sci. Technol.* **26** 015006
[22] Luque A and Ebert U 2010 *Geophys. Res. Lett.* **37** L06806
[23] Liu N, Dwyer J R, Stenbaek-Nielsen H C and McHarg M G 2015 *Nature Comm.* **6** 7540
[24] Qin J and Pasko V P 2015 *Geophys. Res. Lett.* **42** 2031–6
[25] Luque A, Stenbaek-Nielsen H C, McHarg M G and Haaland R K 2016 *J. Geophys. Res. Space Phys.* **121** 2431–49
[26] Liu N Y, Boggs L D and Cummer S A 2016 *Geophys. Res. Lett.* **43** 2635–73
[27] Opaits D F, Shneider M N, Howard P J, Miles R B and Milikh G M 2010 *Geophys. Res. Lett.* **37** L14801
[28] Briels T M P, van Veldhuizen E M and Ebert U 2008 *J. Phys. D: Appl. Phys.* **41** 234008
[29] Ebert U, Montijn C, Briels T M P, Hundsdorfer W, Meulenbroek B, Rocco A and van Veldhuizen E M 2006 *Plasma Sources Sci. Technol.* **15** S118–9
[30] Liu N and Pasko V P 2004 *J. Geophys. Res.* **109** A04301
[31] Ebert U, Nijdam S, Li C, Luque A, Briels T and van Veldhuizen E M 2010 *J. Geophys. Res. Space Phys.* **115** A00E43
[32] Marode E, Bastien F and Bakker M 1979 *J. Appl. Phys.* **50** 140–6
[33] Eichwald O, Yousfi Y, Ducasse O, Merbahi N, Sarette J P, Meziane M and Benhenni M 2011 *Hydrodynamics—Advanced Topics* (London: InTech)
[34] Ono R and Oda T 2004 *Japan J. Appl. Phys.* **43** 321327
[35] Orville R E 1968 *J. Atmos. Sci.* **25** 852–6
[36] Orville R E 1968 *J. Atmos. Sci.* **25** 827–38
[37] Orville R E 1968 *J. Atmos. Sci.* **25** 839–51
[38] Gilmore F R 1955 *RAND Corp., Res. Memo.* **RM-1543** 1–69
[39] Eichwald O, Bayle P, Yousfi Y and Jugroot M 1998 *J. Appl. Phys.* **84** 4704–15
[40] Eichwald O, Bayle P, Yousfi Y and Jugroot M 1998 *J. Appl. Phys.* **84** 4716–26
[41] Kacem S, Ducasse O, Eichwald O, Yousfi M, Meziane M, Sarette J P and Charrada K 2013 *IEEE Trans. Plasma Sci.* **41** 942–7
[42] Liu Q and Zhang Y 2014 *J. Appl. Phys.* **116** 153302
[43] Plooster M N 1970 *Phys. Fluids* **13** 2665–75
[44] Lienard J H IV and Lienard J H V 2008 *A Heat Transfer Textbook* (Cambridge, MA: Phlogiston Press)
[45] Stern M E and Malkus J S 1953 *J. Meteorol.* **10** 105–20
[46] Stern M E 1954 *J. Meteorol.* **11** 495–502
[47] Fleming E F, Jackman C H, Considine D B and Stolarski R S 2001 *J. Geophys. Res. Atmos.* **106** 14245–63
[48] Gumbel J 2001 *J. Geophys. Res.* **106** 10553–63
[49] Kwon K and Park S O 2005 *Fluid Dyn. Conf. Exhib.* **35** 2005–4762 AIAA
[50] Lawson S J and Barakos G N 2011 *Prog. Aerosp. Sci.* **47** 186–216
[51] Gu A and Lim H C 2012 *The Seventh International Colloquium on Bluff Body Aerodynamics and Applications* **7** 244–53
[52] Corda S 2017 *Introduction to Aerospace Engineering with a Flight Test Perspective* (West Sussex: Wiley)
[53] Köhn C, Chanrion O and Neubert T 2017 *Geophys. Res. Lett.* **44** 2604–13
[54] Pasko V P, Inan U S, Bell T F and Taranenko Y N 1997 *J. Geophys. Res.* **102** 4529–61

[55] Chanrion O and Neubert T 2008 *J. Comp. Phys.* **227** 7222–45
[56] Eichwald O and Jugroot M 1996 *J. Appl. Phys.* **80** 694–709
[57] Gardner C S and Shelton J D 1985 *J. Geophys. Res.* **90** 1745–54
[58] Kochkin P O, van Deursen A P J and Ebert U 2015 *J. Phys. D: Appl. Phys.* **48** 025205
[59] Luque A, Ebert U and Hundsdorfer W 2008 *Phys. Rev. Lett.* **101** 075005
[60] Luque A and Ebert U 2014 *New J. Phys.* **16** 013039
[61] Shi F, Liu N Y and Dwyer J R 2017 *J. Geophys. Res.* **122** 10169–76
[62] Luque A, Ratushnaya V and Ebert U 2008 *J. Phys. D: Appl. Phys.* **41** 234005
[63] Naidis G V 2009 *Phys. Rev.* E **79** 057401
[64] Qin J and Pasko V P 2014 *J. Phys. D: Appl. Phys.* **47** 435202
[65] Briels T M P, Kos J, Winands G J J, van Veldhuizen E M and Ebert U 2008 *J. Phys. D: Appl. Phys.* **41** 234004
[66] Ihaddadene M A and Celestin S 2015 *Geophys. Res. Lett.* **42** 5644–51
[67] Cooray V, Arevalo L, Rahman M, Dwyer J R and Rassoul H 2009 *J. Atmos. Sol.-Terr. Phys.* **71** 1890–8
[68] Kochkin P O, van Deursen A P J and Ebert U 2014 *J. Phys. D: Appl. Phys.* **47** 145203
[69] Alekseev G D and Korytov A V 1988 *Nucl. Inst. Met. Phys. Res.* **A268** 151–4
[70] Manders F, Christianen P C M and Maan J C 2008 *J. Phys. D: Appl. Phys.* **41** 234006
[71] Köhn C and Ebert U 2014 *J. Geophys. Res.: Atmos. Phys.* **120** 1620–35
[72] D'Alessandro F 2009 *J. Electrostat.* **67** 482–7
[73] Ariza D F, Montero O R, Román F J and Escobar O F 2011 *International Symposium on Lightning Protection* **11** 101–6
[74] Vogel S and Holbøll J 2017 *Proc. 25th Nordic Insulation Symposium on Materials, Components and Diagnostics* (https://doi.org/10.5324/nordis.v0i25.2353)
[75] Reddy K P J and Sharath N 2013 *Curr. Sci.* **104** 172–6
[76] Surana K S, Reddy K P J, Joy A D and Reddy J N 2014 *Int. J. Comp. Fluid Dyn.* **28** 251–7